ADVANCED ENERGY MATERIALS
www.advenergymat.de

On the Practical Applicability of the Li Metal-Based Thermal Evaporation Prelithiation Technique on Si Anodes for Lithium Ion Batteries

Egy Adhitama, Marlena M. Bela, Feleke Demelash, Marian C. Stan, Martin Winter, Aurora Gomez-Martin,* and Tobias Placke*

Lithium ion batteries (LIBs) using silicon as anode material are endowed with much higher energy density than state-of-the-art graphite-based LIBs. However, challenges of volume expansion and related dynamic surfaces lead to continuous (re-)formation of the solid electrolyte interphase, active lithium losses, and rapid capacity fading. Cell failure can be further accelerated when Si is paired with high-capacity, but also rather reactive Ni-rich cathodes, such as $LiNi_{0.8}Co_{0.1}Mn_{0.1}O_2$ (NCM-811). Here, the practical applicability of thermal evaporation of Li metal is evaluated as a prelithiation technique on micrometer-sized Si (µ-Si) electrodes in addressing such challenges. NCM-811 || "prelithiated µ-Si" full-cells (25% degree of prelithiation) can attain a higher initial discharge capacity of ≈192 mAh $g_{NCM\text{-}811}^{-1}$ than the cells without prelithiation with only ≈160 mAh $g_{NCM\text{-}811}^{-1}$. This study deeply discusses significant consequences of electrode capacity balancing (N:P ratio) with regard to prelithiation on the performance of full-cells. The trade-off between cell lifetime and energy density is also highlighted. It is essential to point out that the phenomena discussed here can further guide the direction of research in using the thermal evaporation of Li metal as a prelithiation technique toward its practical application on Si-based LIBs.

1. Introduction

Lithium-ion batteries (LIBs) have revolutionized human civilization as they have laid the foundation of portable electronic devices, electric vehicles, and renewable energy toward a fossil fuel-free society.[1,2] Further developments in the whole battery value chain and across all technology readiness levels are needed to fulfill the demand for batteries with increased energy density and fast charging capability, lower cost, and higher safety.[3,4] With regard to the negative electrode (anode), so-called "alloying-type" materials such as tin and silicon have become promising candidates to replace state-of-the-art (SOTA) graphite in future LIBs because they can reversibly store nearly four lithium ions per host atom offering much higher energy densities.[5–7] Si has become more attractive than Sn most likely due to the lower cost, greater availability, and higher capacity.[8–10] In theory, the specific capacity that can be achieved with Si is up to 3579 mAh g^{-1} combined with a low average delithiation potential (≈0.4 V vs $Li|Li^+$) and low voltage hysteresis.[11] Despite all these advantageous characteristics, the practical use of Si-based anode materials in commercial LIB cells faces major challenges, i.e., enormous particle stress on the atomic scale which leads to particle fracture and detachment from the current collector on the electrode scale.[12] In addition, continuous (re-)formation of the solid electrolyte interphase (SEI) causes ongoing active lithium losses (ALL) and

E. Adhitama, M. M. Bela, F. Demelash, M. C. Stan, M. Winter, A. Gomez-Martin, T. Placke
MEET Battery Research Center
Institute of Physical Chemistry
University of Münster
Corrensstr. 46, 48149 Münster, Germany
E-mail: egyadhitama@uni-muenster.de; agomezma@uni-muenster.de

The ORCID identification number(s) for the author(s) of this article can be found under https://doi.org/10.1002/aenm.202203256.

DOI: 10.1002/aenm.202203256

E. Adhitama
International Graduate School for Battery Chemistry, Characterization, Analysis, Recycling and Application (BACCARA)
University of Münster
Corrensstr. 40, 48149 Münster, Germany

M. Winter
Helmholtz Institute Münster
IEK-12
Forschungszentrum Jülich GmbH
Corrensstr. 46, 48149 Münster, Germany

electrolyte consumption making the practical application even more challenging.[13–15]

The quest to achieve maximum use of Si in the anode is lengthy and despite various efforts that have been made in recent years, several challenges still remain. Strategies have been devoted to the modification of the Si particle morphology and size to prevent particle cracking during cycling.[16–18] Several attempts to develop advanced electrolytes enabling an effective SEI formation have also been pursued.[19–21] Recently, prelithiation has become a quite popular approach in the battery community to compensate for ALL.[22–25] In SOTA LIB cells, the active Li source is limited by the positive electrode (cathode). Part of the available active Li then will be consumed to form the SEI at the anode|electrolyte interface during the first (few) charge/discharge cycles of the cell. To some extent, if the SEI continuously grows, the active Li will also be continuously consumed, thereby further decreasing the amount of active Li content left so that the cell will subsequently experience fast capacity fading.[26] The role of prelithiation is to compensate for these ALL in the 1st cycle (or first few cycles) by adding a certain amount of extra active Li to the battery cell prior to operation.[22,27,28] In addition, the prestored Li can also act as a reservoir of active Li to address ongoing ALL during cycling.[29,30]

To date, the most commonly employed prelithiation technique is direct contact prelithiation of the anode by using passivated Li metal powder due to its simplicity.[31–33] However, the inhomogeneous Li distribution within the electrode should be taken into account when applying this technique,[34] as the cells will experience self-discharge and unintentional aging behavior.[35] To overcome these issues, we recently developed a Li thermal evaporation technique on Si thin films to facilitate uniformly lateral and in-depth Li distributions.[35] Prelithiation by Li thermal evaporation overcomes the above-mentioned challenges using passivated Li metal powder, i.e., avoiding direct handling with Li metal powder, the ability to precisely control the degree of prelithiation, and ensuring highly homogeneous Li metal distribution at the electrode surface.[34] In our previous study, the capacity retention was notably improved with up to 70% state-of-health after 200 cycles due to "pre-SEI formation" and homogeneous Li-Si alloying reaction.[35] However, only Si thin films were investigated as model electrode systems and electrochemical analysis was only performed in Si || Li metal cells with a large excess of active Li inventory. Therefore, its suitability in realistic electrodes and/or realistic cells (e.g., by using powder-based Si electrodes in an LIB full-cell setup) remains an open question.

Here, the practical applicability of the Li metal-based prelithiation technique in powder-based Si electrodes was evaluated. The Li thermal evaporation technique was used to deposit Li metal (with the desired thickness of ≈1 µm) on micrometer-sized Si electrodes (further abbreviated as "preLi µ-Si"). The electrodes were evaluated in both Li metal cells and a full-cell setup (against $LiNi_{0.8}Co_{0.1}Mn_{0.1}O_2$ (NCM-811)) in two-electrode and three-electrode configurations as it is necessary to evaluate practical relevance and for a more comprehensive electrochemical analysis.[36,37] The use of the Si-based anode in combination with Ni-rich NCM-811 as cathode material in this study is of great importance as these materials have the potential to boost the energy density of LIBs to meet increasing demands for high-energy applications.[38]

We also discussed Li utilization (degree of prelithiation) and distribution as it is highly affected by the physical properties of the active anode materials (e.g., particle size and surface area).[39] The use of "µ-Si" opens up the possibility to understand the depth of lithiation as it might affect the failure mechanism of Si-based cells. We investigated different electrode capacity balancing (N:P ratio) and its trade-off with energy density. Finally, it is essential to point out that the phenomena discussed in this study can further navigate the direction of research in using the thermal evaporation of Li metal as a prelithiation technique toward its practical application on powder-based Si anodes.

2. Results and Discussion

2.1. Investigation on Li Utilization (= Degree of Prelithiation)

As the first point of interest, the Li utilization (degree of prelithiation) was investigated as it is highly influenced by the particle size and specific surface area of the active materials. Scanning electron microscopy (SEM) images of "µ-Si" before and after Li metal deposition in the dry state (without electrolyte exposure) are shown in Figure S1a,b in the Supporting Information, revealing similar morphological features. In pristine conditions, "µ-Si" electrodes show a rugged surface structure with a particle size of ≈2–5 µm (Figure S1a, Supporting Information). After Li deposition (≈1 µm) by thermal evaporation technique, the vapor-deposited Li metal is not visible indicating that Li

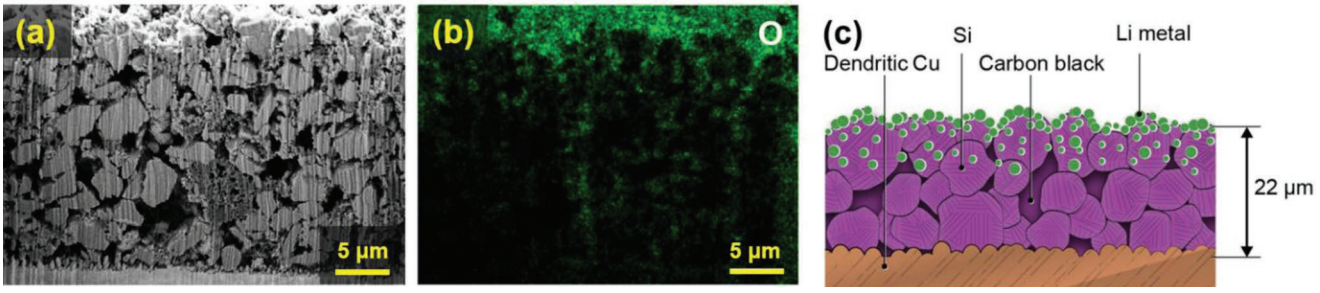

Figure 1. a) Cryo-FIB cross-section images of the "preLi µ-Si" electrode (≈1 µm deposited Li metal). b) Corresponding elemental mapping of oxygen (O) which is shown in (a) by EDX. c) Schematic illustration of the Li deposition by thermal evaporation on "preLi µ-Si". The experiments were conducted in the dry state (without electrolyte addition).

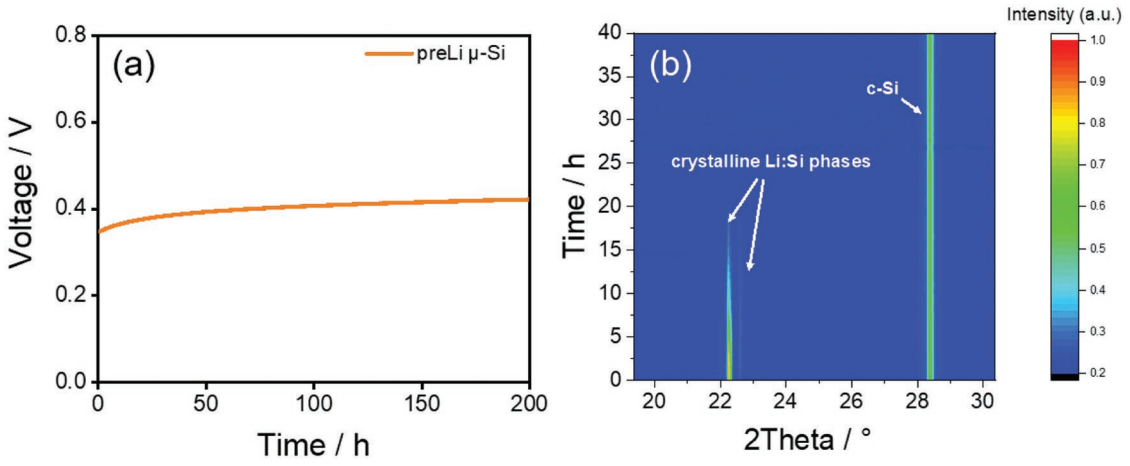

Figure 2. a) OCV development of "preLi µ-Si" || Li metal cells for 200 h resting time. b) In situ XRD analysis of "preLi µ-Si" electrodes at OCV condition (the corresponding phases are labeled accordingly). The experiments were conducted after the addition of electrolytes (wet state).

metal is not accumulated on the electrode surface (Figure S1b, Supporting Information). Cryo-focused-ion beam (FIB) combined with energy-dispersive X-ray spectroscopy (EDX) measurements were then performed at –150 °C to further prove the presence and distribution of vapor-deposited Li metal without damaging it (**Figure 1**a,b). Once Li metal is deposited, a thin layer will be formed at the Li metal|air interface which is rich in oxygen (O) suggesting a combination of Li_2CO_3/Li_2O.[35] For this reason, the corresponding EDX analysis for the element O is provided to indicate the presence of Li metal. From Figure 1b, it can be seen that Li metal is well-distributed not only at the top part particle level but also highly uniform at the overall electrode level. However, one should note that the presence of Li becomes less evident on the current collector side. The illustration of this phenomenon is depicted in Figure 1c. To give further evidence of this uniformity, we also deposited ≈1 µm of Li metal by thermal evaporation technique on the Si wafer. The cryo-FIB combined with EDX results as shown in Figure S2a–c in the Supporting Information clearly confirm a highly uniform Li metal deposition on top of the Si wafer, which illustrates what happened in the case of the "µ-Si" electrode right after Li metal deposition.

After Li thermal evaporation, the lithiation step in "preLi µ-Si" was evaluated by performing a galvanostatic discharge experiment. From now on, the electrolyte is involved in the experiments (further referred to as the "wet state"). Figure S3a,b in the Supporting Information shows that the deposited 1 µm thick Li metal is not able to fully lithiate "µ-Si" electrodes, meaning 1 Si atom only alloys with ≈0.97 atoms of Li which corresponds to a capacity of 934 mAh g^{-1} ($Li_{0.97}Si$ or ≈25% degree of prelithiation). The reason behind this phenomenon might be because the "preLi µ-Si" electrodes have a high specific surface area (3.42 m^2 g^{-1}) and a notable electrode thickness (≈22 µm) with high porosity.[39]

To gain a better understanding of how deposited Li metal lithiates the "µ-Si," the open-circuit voltage (OCV) of "preLi µ-Si" was held up to 200 h as shown in **Figure 2**a. The relatively high initial OCV of 0.4 V suggests that the deposited Li metal might only cover the top layer of the "µ-Si" particles, which results in incomplete lithiation. Based on this observation, one would expect that there will be no formation of crystalline (c-)$Li_{15}Si_4$ as this phase is only formed at potentials between 0.05 and 0.07 V.[6,40] However, phase evolution examination using in situ X-ray diffraction (in situ XRD) as shown in Figure 2b seems to point to a different conclusion. Two reflections at $2\theta \approx 22.3°$ and $2\theta \approx 22.6°$ suggest the presence of the c-$Li_{15}Si_4$ phase and other c-Li_xSi_y phases.[41] This observation is further supported by Figure S4 in the Supporting Information where a sharp peak exists at ≈0.45 V in the differential capacity (dQ/dV) versus voltage profile during delithiation, indicating the existence of the c-$Li_{15}Si_4$ phase and its transformation to an amorphous phase during delithiation.[40] Figure 2b also shows that the XRD reflection of the c-$Li_{15}Si_4$ phase is then gradually diminished over time indicating the self-discharge process as Li reacts with electrolyte to form the SEI. The fact that c-Si at $2\theta \approx 28.6°$ still exists after the disappearance of c-$Li_{15}Si_4$ and does not transform to amorphous a-Si is counter-intuitive to what is typically reported in the literature.[42] This different behavior is probably because the lithiation happens only on the top layer of the electrode and cannot fully lithiate all "µ-Si" particles within the electrode.

2.2. Designing Suitable Capacity Balancing (N:P Ratio) with Regard to Prelithiation

An important factor that can influence cell performance is the negative electrode (anode) to positive electrode (cathode) capacity balancing ratio (N:P ratio).[36] It is widely reported that the optimum N:P value is ≈1.03–1.20 to get the right balance between high energy density and high safety.[43,44] However, this is particularly true for the SOTA LIBs technology (i.e., cells comprising graphite as an anode). Under special circumstances, for instance, the use of Si as the anode, this electrode balancing becomes an open question as the material's stability and lithiation degree might be influenced by the N:P ratio and thus become an area to be explored further. Furthermore, with regard to prelithiation, there is preserved capacity from predeposited Li metal that should be taken into account to determine the N:P ratio, which is also known as a safety factor.[45] In Si-based LIB cells, apart from Li metal plating, the

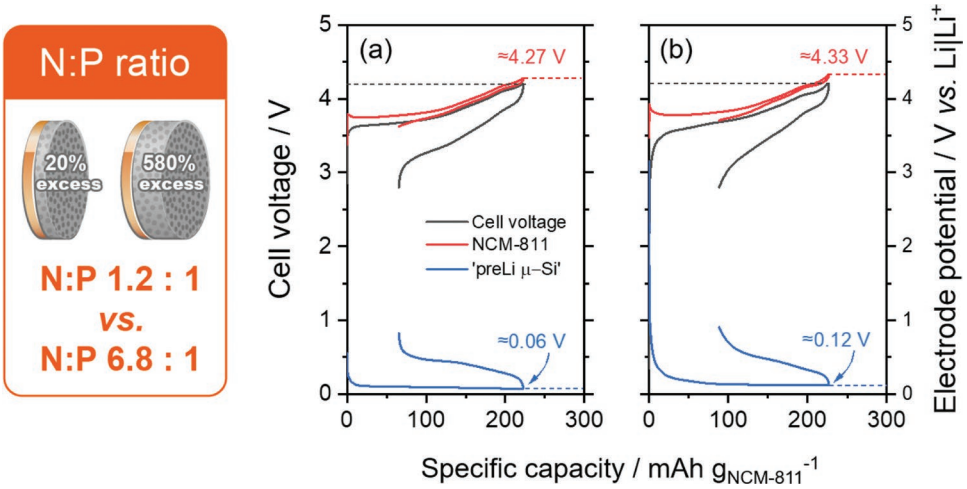

Figure 3. First cycle cell voltage and individual potential profiles of each electrode in NCM-811 || "preLi μ-Si" full-cells with a) N:P ratio of 1.2 and b) N:P ratio of 6.8. The cutoff voltages were 2.8–4.2 V, with a constant voltage (CV) step during charge until the specific current reached values below 0.05 C (1 C = 190 mA g^{-1}).

right choice of the N:P ratio is also critical to avoid the occurrence of the highest lithiated c-$Li_{15}Si_4$ phase and thus severe volume changes. However, it is important to point out that the value of the N:P ratio might only be true for the 1st cycle as it is a dynamic value due to parasitic (lithium-consuming) reactions.[46] In this chapter, the impact of an N:P ratio in prelithiated cells with a contrast value (1.2 vs 6.8, not considering the additional lithium from prelithiation) is evaluated, in particular, how it can influence the (de-)lithiation process. Therefore, a full-cell setup in a three-electrode configuration (Swagelok cell) was employed as this configuration allows monitoring of the individual electrode potentials of the N and P electrodes at the same time.[36]

An overview of the end-of-charge (EOC) and end-of-discharge (EOD) potentials for the "preLi μ-Si" and NCM-811 electrodes is given in **Figure 3**a,b and **Table 1**. In an ideally balanced full-cell setup, the electrode potentials can be indirectly adjusted by precise selecting of the cell cutoff voltages and balancing of negative electrode (N):positive electrode (P) capacities (N:P ratio)—at least for the first charge/discharge cycle. During cycling, the electrode potentials evolve and can be shifted as a result of parasitic side reactions (e.g., consumption of active Li). Therefore, in both cases, either in the cells with an N:P ratio of 1.2 or 6.8, the potential evolved where the shift occurred to higher potentials for the cathode and the anode during cycling, which is a result of active Li losses (ongoing SEI formation). Therefore, the anode will be less lithiated in the ongoing cycles. However, there is a slightly noticeable difference where in the cells with an N:P ratio of 1.2, the EOC anode stops at 0.06 V meanwhile in the cells with an N:P ratio of 6.8, the EOC anode stops at 0.12 V (Figure 3a,b). This leads to a different depth of lithiation. In more detail, Figure S5a,b in the Supporting Information show "μ-Si" potential (vs Li|Li^+) as a function of specific capacity calculated by the mass of its active materials. In the cell with an N:P ratio of 1.2, the Li utilization reaches 2774 mAh $g_{\mu\text{-}Si}^{-1}$ while in the cell with an N:P ratio of 6.8, the Li utilization reaches 1893 mAh $g_{\mu\text{-}Si}^{-1}$, respectively. To understand this process better, Figure S5c in the Supporting Information shows the summary of the potential profile of "μ-Si" versus Li|Li^+ in the full-cells with different N:P ratios at the EOC.

Taking a deeper look at the dQ/dV versus voltage profile of the anode in this full-cell setup, the cell with an N:P ratio of 1.2 shows the characteristic peak of c-$Li_{15}Si_4$ at 0.45 V during delithiation (Figure S6, Supporting Information). As previously reported, the formation of c-$Li_{15}Si_4$ has been linked to an increased capacity loss upon cycling due to the dynamic change and disconnection of Si materials.[42] For long-term cycling, the formation of c-$Li_{15}Si_4$ entailing severe volume changes will be a critical issue. To further demonstrate the impact of cell balancing in prelithiated cells, the cell with a balancing of 1.2 shows worse Initial Coulombic efficiency (IC_{Eff}) and worse delithiation capacity in the first cycle as compared to the cells with a balancing of 6.8 (Figure S7, Supporting Information). These results were caused by a higher lithiation and thus larger volume changes of the "μ-Si" when it is assembled in the cells with a balancing of 1.2 than to 6.8. In the long-term, it results in enhanced capacity fading, electrolyte decomposition and increased ALL as can be seen from the voltage profile, normalized capacity, and accumulated Coulombic inefficiency

Table 1. First cycle end-of-charge (EOC) and end-of-discharge (EOD) cell voltages and electrode potentials (in V vs Li|Li^+) of the positive (NCM-811) and the negative electrode ("preLi μ-Si") within the cell voltage range 2.8–4.2 V.

N:P balancing ratio	EOC cell [V]	EOC anode [V] versus Li|Li^+	EOC cathode [V] versus Li|Li^+	EOD cell [V]	EOD anode [V] versus Li|Li^+	EOD cathode [V] versus Li|Li^+
1.2 : 1.0	4.2	0.06	4.27	2.8	0.9	3.62
6.8 : 1.0	4.2	0.12	4.33	2.8	0.8	3.70

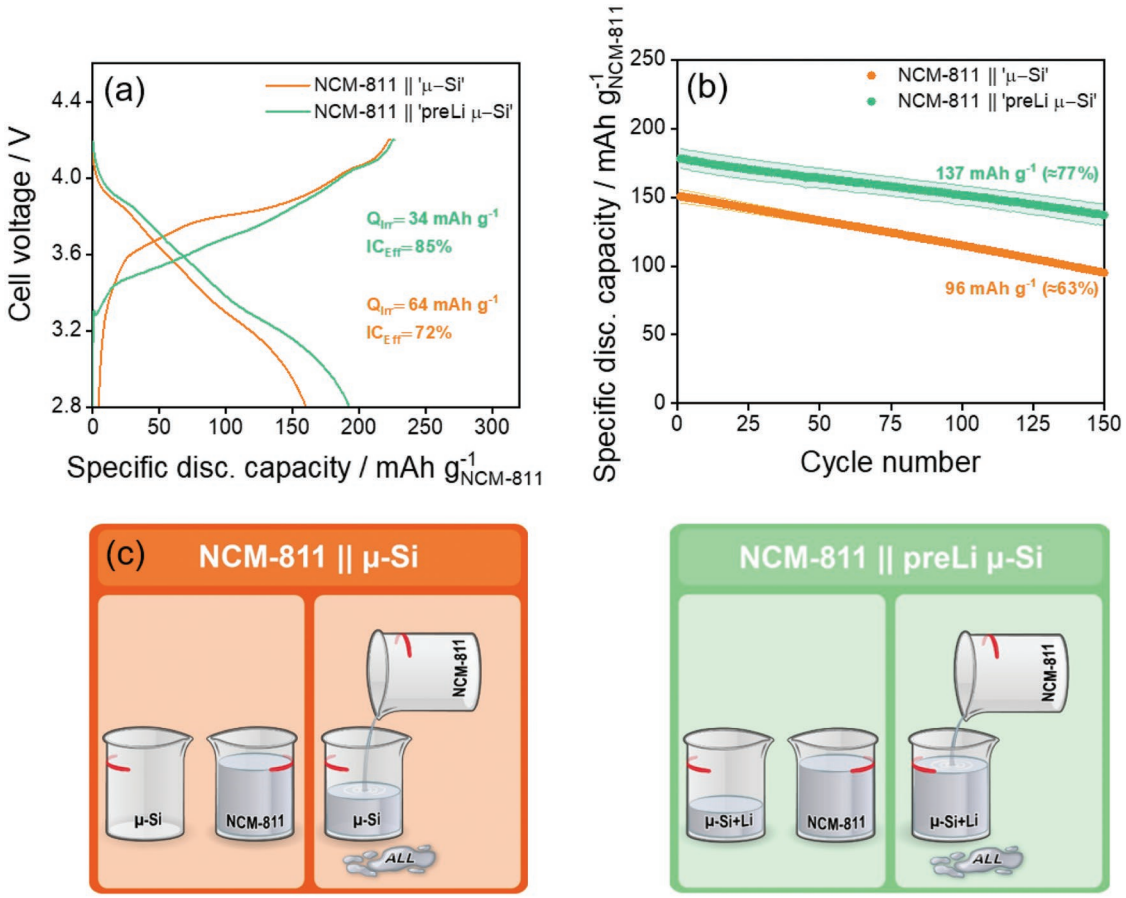

Figure 4. a) First cycle cell voltage profiles of the two NCM-811 || "μ-Si" cells at 0.1 C in a cell voltage range of 2.8–4.2 V. b) Long-term stability profile at 0.33 C (1 C = 190 mA $g_{NCM\text{-}811}^{-1}$) with an N:P ratio of 6.8. At least three cells were tested for each cell sample to ensure high reproducibility. c) Schematic illustration to describe the concepts of active lithium loss (ALL) and the compensation by prelithiation.

(ACI) profiles in Figure S8a–d in the Supporting Information. Based on the course of these observations, the used N:P ratio of 6.8 seems to be a "safer" choice in terms of an extended lifetime as it should not result in a severe capacity loss and therefore will be used in the next chapter. Further discussions on the trade-off between cycling stability versus energy density are given in the last chapter.

2.3. Long-Term Cycling Stability Observations in NCM-811 || "preLi μ-Si" Cells

The full-cell cycling performance with an N:P ratio of 6.8 for pristine and prelithiated μ-Si electrodes is discussed in this chapter. The cells were first cycled at 0.1C for four cycles. **Figure 4**a shows the notable impact of prelithiation to minimize capacity loss/Q_{irr} (from 64 mAh $g_{NCM\text{-}811}^{-1}$ to 34 mAh $g_{NCM\text{-}811}^{-1}$) and to enhance C_{Eff} (from 72% to 85%) in the 1st cycle. The NCM-811 || "preLi μ-Si" cells could deliver a delithiation capacity of 192 mAh $g_{NCM\text{-}811}^{-1}$ which is notably higher than that of NCM-811 || "μ-Si" cells that attained a delithiation capacity of only 160 mAh $g_{NCM\text{-}811}^{-1}$. This confirms that ALL is suppressed during the formation of SEI in the initial cycles by prelithiation (Figure S9, Supporting Information).

Differential capacity versus voltage plots corroborates the high capacity gained for NCM-811 || "preLi μ-Si" cells. The dQ/dV profiles as a function of the cell voltage in the 1st cycle are shown in Figure S10 in the Supporting Information. The small hump at 3.25–3.50 V in NCM-811 || "μ-Si" cells is due to SEI formation while this is not the case for NCM-811 || "preLi μ-Si" cells as the SEI has been formed prior to the battery cell operation. The SEI was preformed during the resting period as the electrolyte was in contact with "preLi μ-Si" electrodes. The first two oxidation peaks of NCM-811 || "preLi μ-Si" cells are also a bit shifted to lower voltages (≈3.52 and 3.65 V) indicating that the multiphase transitions happened earlier. This is probably because the "preLi μ-Si" active materials have already been activated so that the alloying reaction happens faster and therefore enhances the reversibility (lower Q_{irr}). These features are similar to the dQ/dV versus voltage profile comprising NCM-811 || Li metal cells.[47]

A notable difference in long-term cycling stability was also detected as shown in Figure 4b. After 150 cycles, the NCM-811 || "μ-Si" cells show a rapid capacity fade to 96 mAh $g_{NCM\text{-}811}^{-1}$ whereas NCM-811 || "preLi μ-Si" cells could deliver a capacity of 137 mAh $g_{NCM\text{-}811}^{-1}$. In terms of C_{Eff}, NCM-811 || "preLi μ-Si" cells achieved substantially higher mean C_{Eff} of 99.6% and better capacity retention of 77% compared to NCM-811 || "μ-Si"

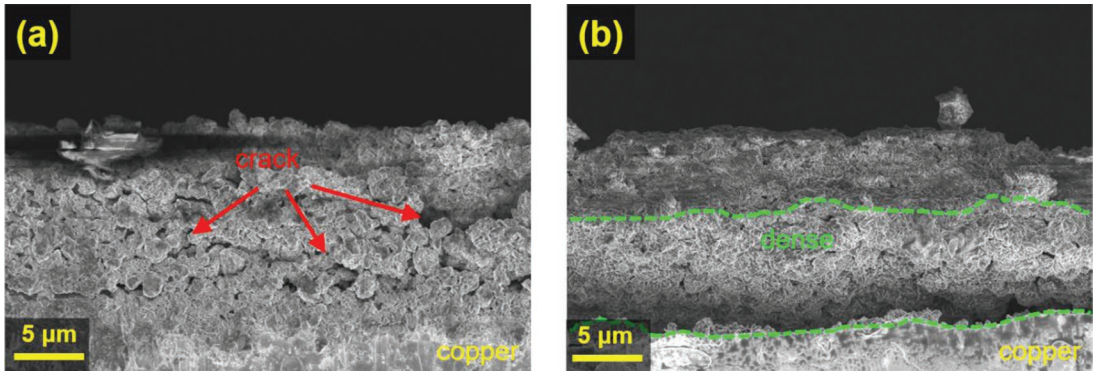

Figure 5. Side-view SEM images of µ-Si anodes after 150 cycles in a) NCM-811 || "µ-Si" and b) NCM-811 || "preLi µ-Si" cells.

cells with a mean C_{Eff} of 99.4% and capacity retention of 63% (mean C_{Eff} is calculated by excluding preconditioning cycles), respectively. In line with this finding, the ACI of prelithiated cells was remarkably lower than non-prelithiated cells as depicted in Figure S11 in the Supporting Information.

After 150 cycles, cycled electrodes were retrieved from the cells in discharged states and analyzed via cross-section SEM. As can be seen in **Figure 5**, the "µ-Si" electrodes show numerous visible cracks while "preLi µ-Si" remains uniform and dense. A possible mechanism why prelithiated cells outperform non-prelithiated cells (e.g., higher attainable capacity, higher capacity retention, lower ACI) can be attributed to three factors: I) tailored pre-SEI formation,[35] II) compensation of ALL in initial cycles, and III) additional Li from the reservoir. This compensation of ALL in initial cycles is schematically illustrated in Figure 4c.

2.4. Fair Evaluation and Final Remarks: Trade-Off between Cycling Stability versus Energy Density

Results of this study have proven that "preLi µ-Si"-based anodes in full-cell configuration against an NCM-811 cathode show an outstanding initial specific capacity, capacity retention, and C_{Eff} compared to their counterparts using "µ-Si" anode without prelithiation. While it is true that this approach can compensate for initial and ongoing ALL, nonetheless, it still cannot exploit the maximum use of Si as it hardly solves its main challenge, namely volume expansion. This is further proven in Figure S8d in the Supporting Information. Even with the help of prelithiation, the high utilization of Si capacity (N:P ratio of 1.2) leads to tremendous ACI originating from Si particle cracking, SEI (re-) formation, and ALL. The higher utilization of Si capacity comes with a higher tendency of continuous electrolyte decomposition, electronic disconnection of Si active materials, and possibly trapped Li.[48] On the contrary, lower capacity utilization of Si (e.g., with an N:P ratio of 6.8) is, on the one hand, beneficial to reduce the volume changes for an improved lifetime, especially at increased applied currents, however, will also result in substantially decreased energy density.

In more detail, Table S1 in the Supporting Information presents an approach for the calculation of the specific energy on the active material level of the cells using an N:P ratio of 1.2 and 6.8. Due to the difficulty in taking into account the dynamic changes of Si particles upon cycling, the specific energy was only calculated based on the 1st cycle. The specific energy on the active material level was calculated from the mean cell discharge voltages, practical specific discharge capacities of the cathode, and the areal mass loading of both cathode and anode which is associated with its N:P ratio according to our previous study.[49] A higher specific energy value (514 Wh kg^{-1}) is obtained for NCM-811 || "preLi µ-Si" cells with an N:P ratio of 1.2 at expense of poor stability. On the other hand, the obtained specific energy of the NCM-811 || "preLi µ-Si" cells with an N:P ratio of 6.8 is slightly lower (387 Wh kg^{-1}) which is compensated by better stability. Nevertheless, this obtained specific energy is still higher than SOTA graphite-based cells. Based on these simple calculations, one can say that Si has the promise to push the limit of LIBs energy density, but the path for its practical applications still needs further improvements. There should be an alternative to compromising this sweet spot (cycling stability vs energy density). The option of using Si/graphite composites with lower Si contents and controlled physical properties should result in better performance and should be evaluated in terms of prelithiation in future studies.

The battery performance discussed here has been evaluated in two-electrode coin cells and three-electrode Swagelok cell setups. For more practical two-electrode cell formats, the use of multilayer pouch cells with optimized electrochemical testing conditions is necessary. Finally, the study discussed here reaffirms the promise of the thermal evaporation of Li metal as it outperforms other prelithiation techniques utilizing Li metal (Table S2, Supporting Information). It plays an important role to overcome ALL in powder-based Si anodes. The pretreatment technique enables a mean C_{Eff} of 99.6% and capacity retention of ≈77% (137 mAh $g_{NCM\text{-}811}^{-1}$) after 150 cycles against an NCM-811 cathode. We believe that this work can serve as an essential study to navigate future research direction and further advance Si anodes, offering a pathway to practical application with regard to the prelithiation technique.

3. Conclusion

A systematic evaluation of the practical applicability of the Li metal-based thermal evaporation prelithiation technique on Si anodes is thoroughly discussed in this study. The practical relevance was examined by evaluating the cells in Li metal cells and a full-cell setup (consisting of NCM-811 as a cathode and µ-Si as

an anode) in two-electrode and three-electrode configurations for a more comprehensive electrochemical analysis. The different electrode capacity balancing (N:P ratio) was deeply investigated where an N:P ratio of 1.2 leads to severe capacity loss, and therefore, the N:P ratio of 6.8 is chosen as a "safer" choice. It was shown that NCM-811 || prelithiated µ-Si full-cells (25% degree of prelithiation) can attain a higher initial discharge capacity of ≈192 mAh $g_{NCM\text{-}811}^{-1}$ with better capacity retention of 77% than the cells without prelithiation with only 160 mAh $g_{NCM\text{-}811}^{-1}$ and 63% capacity retention. The remark on the trade-off between cell lifetime and energy density with regard to the prelithiation was highlighted. The calculation of the specific energy on the active material level is presented and compared to SOTA graphite-based LIB cells. While it is true that the prelithiation approach can compensate for initial and ongoing ALL, nonetheless, it is still unable to solve its main challenge (i.e., volume expansion). Nevertheless, the phenomena discussed in this study shall provide certain guidance to the research in using the thermal evaporation of Li metal as a prelithiation technique on Si anodes to reach the point in the future when the optimum cell system comprising Si as an anode can be applied (i.e., the use of N:P ratios of 1.03–1.2) without sacrificing the stability.

4. Experimental Section

Electrode Preparation: The negative electrode was comprised of a commercial micrometer-sized Si active material (Brunauer–Emmett–Teller (BET) surface area = 3.42 $m^2\ g^{-1}$; d_{50} = 2.72 µm, d_{90} = 5.4 µm), a conductive agent (Super C65, *Imerys Graphite and Carbon*), and as binders polyacrylic acid (*Sigma-Aldrich;* average Mv 450000) which was lithiated by mixing with LiOH (*Sigma-Aldrich,* purity: 99.5%) and sodium-carboxymethyl cellulose (Walocel CRT 2000 PPA12, *Dow Wolff Cellulosics*) with a ratio of 85, 5, 2.3, and 7.7 wt%, respectively. Deionized water was used as a solvent and all materials were homogenized by a planetary centrifugal mixer (ARM-310CE, *Thinky Corporation*) at a speed of 1700 rpm for 45 min in total. The anode paste was coated on dendritic copper foil (*Schlenk*; thickness: 20 µm) with a doctor-blade (*Zehntner GmbH*) with a gap of 50 µm and an automatic film applicator (*Sheen Instruments*). The electrode sheets were dried for 2 h at 80 °C and the electrode thickness was shrunk to ≈22 µm. After predrying at 80 °C, the sheets were dried in an oven at 90 °C for 10 h under reduced pressure. Circular electrode disks with Ø = 15 mm in diameter were punched out for two-electrode coin cells and Ø = 12 mm for Swagelok cell investigations. The average active mass loading of the anodes was i) ≈1.02 ± 0.16 mg cm^{-2}, resulting in an areal capacity of ≈3.08 ± 0.50 mAh cm^{-2} for the cell with an N:P ratio of 1.2 and ii) ≈1.53 ± 0.03 mg cm^{-2}, resulting in an areal capacity of ≈5.52 ± 0.14 mAh cm^{-2} for the cell with an N:P ratio of 6.8 (calculated based on the practical capacity of the Si ≈3000 mAh g^{-1}).

The positive electrodes consisted of 94 wt% NCM-811 ($LiNi_{0.8}Mn_{0.1}Co_{0.1}O_2$, *Jiangmen KanHoo Industry Co., LTD;* BET surface area = 0.30 – 0.90 $m^2\ g^{-1}$, d_{50} = 3.38 µm, d_{90} = 6.89 µm) as active material, 3 wt% carbon black as conductive agent (Super C65, *Imerys Graphite and Carbon*) and 3 wt% PVdF as a binder (Solef 5130, *Solvay*). *N*-methyl-2-pyrrolidone (anhydrous, purity: 99.5%, *Sigma-Aldrich*) was used as the solvent with a solid content of 50 wt%. The electrode paste was then homogenized by a planetary centrifugal mixer at a speed of 1700 rpm for 15 min and 500 to 700 rpm for 5 min. After mixing, the electrode paste was coated with a doctor-blade and an automatic film applicator on aluminum foil (20 µm, *Nippon foil*) which was previously washed with ethanol. The electrode sheets were dried for 2 h at 80 °C and calendered (CLP 2025, *Hohsen Corp.*) to reach a porosity of 35%.

The NCM-811 electrode sheets were then punched out with Ø = 14 mm in diameter (for two-electrode coin cell investigations) and Ø = 12 mm in diameter (for three-electrode Swagelok cells), followed by drying in a Büchi B-585 glass oven under reduced pressure (<$5{\cdot}10^{-2}$ bar) for 8 h at 90 °C. The average areal capacities of the NCM-811 electrode were i) ≈2.35 ± 0.01 mAh cm^{-2} (mass loading of ≈12.41 ± 0.03 mg cm^{-2}) for the cell with an N:P ratio of 1.2. For the cell with an N:P ratio of 6.8, ii) the average areal capacities were ≈0.81 ± 0.04 mAh cm^{-2} (mass loading of ≈4.28 ± 0.04 mg cm^{-2}). All mass/capacity values were calculated based on the NCM-811 practical capacity of 190 mAh g^{-1} in NCM-811 || Li-metal cells considering an upper cutoff potential of 4.20 V versus $Li|Li^+$.

Prelithiation of µ-Si Negative Electrodes by Thermal Evaporation: µ-Si electrode sheets were deposited with Li metal by using the physical vapor deposition (PVD) method, i.e., the so-called Li thermal evaporation, as reported in the previous publication.[35] The PVD system (ProVap 3G) is integrated with an Ar-Glovebox (*MBraun*). The H_2O and O_2 levels were controlled below 0.1 ppm. The deposition process was controlled by an SQC-310 quartz crystal controller (*Inficon GmbH*) and a quartz crystal microbalance (QCM) crystal sensor (6 MHz). The µ-Si electrode was fixed on a rotating sample holder inside the evaporation chamber and then the chamber was evacuated until a pressure of 10^{-6} mbar. Li metal pellets were placed in a Tantalum boat source and the evaporation occurred at a constant deposition rate of 5 Å s^{-1} (power increased to 25%). Prior to the experiment, the glove box was purged several times with fresh Ar and the box was baked out several times with a heat gun at 200 °C to minimize contamination. Once the desired thickness of 1 µm was achieved (≈25% degree of prelithiation based on the specific capacity of Si anode), the samples were transferred to an air-tight sample holder for further experiments to avoid air exposure.

Cell Assembly and Electrochemical Investigation: Electrochemical investigations were first carried out in a three-electrode configuration[36] in T-cells (*Swagelok*, custom in-house design) to find a suitable N:P balancing ratio and to determine the evolution of individual potentials of both positive and negative electrodes upon cycling. The inside body of the Swagelok cell was previously covered with an insulating Mylar foil (polyethylene terephthalate). Five-layered polyolefin Freudenberg FS2190 disks were used as separators (*Freudenberg*) with a size of Ø = 13 mm and Ø = 8 mm soaked with 120 and 60 µL electrolyte, respectively (battery-grade 1 M lithium hexafluorophosphate ($LiPF_6$) in ethylene carbonate/ethyl methyl carbonate (3:7 by weight) with 10 wt% fluoroethylene carbonate as SEI-forming additive; *BASF SE*). NCM-811 (Ø = 12 mm) and µ-Si (Ø = 12 mm) electrodes and Li metal (Ø = 8 mm) were used as positive, negative, and reference electrodes, respectively.

A two-electrode configuration[36] in CR2032 coin cells (*Hohsen Corporation*) was employed to elucidate the degree of prelithiation and long-term cycling stability. In Li metal cells (both µ-Si || Li metal and NCM-811 || Li metal cells), Li metal foil (Ø = 15 mm) with 500 µm in thickness (battery grade: purity ≥99.9%, *China Energy Lithium* (*CEL Co.*)) was used as a negative electrode paired with µ-Si or NCM-811 as positive electrodes (Ø = 14 mm). A Ø = 16 mm separator (Celgard 2500, polypropylene) was placed between the two electrodes. All cells were filled with 50 µL electrolyte. For NCM-811 || µ-Si-based full-cells, two-layered polyolefin Freudenberg FS2190 disks were used as separators (*Freudenberg*) with a size of Ø = 16 mm soaked with 100 µL electrolyte. The diameter of NCM-811 was Ø = 14 mm while the diameter of µ-Si was Ø = 15 mm.

Constant current constant voltage charge–discharge electrochemical experiments were performed on a Maccor Series 4000 battery tester (*Maccor, Inc.*) at 20 °C. All cells had a rest period of 6 h at OCV unless stated otherwise. For Li metal cells, the cells were cycled in a voltage range of 0.05–1.20 V. For the full-cell setup, the cells were charged to 1.5 V for 15 min prior to 6 h at OCV to avoid Cu current collector dissolution.[50] Cells were then cycled for four cycles at 0.1 C to stabilize the interphase, followed by cycling at 0.33 C for 150 cycles (1 C = 190 mA g^{-1}) within the voltage range of 2.8–4.2 V, respectively. For the investigation using Swagelok cells, two cells of each sample were performed and for the investigation using coin cells, at least the samples were repeated three times to ensure a sufficiently high reproducibility.

Characterization Methods: The morphology of the electrodes was characterized using a SEM (Carl Zeiss AURIGA; *Carl Zeiss Microscopy*

GmbH). SEM images were taken using a working distance between 3.5 and 4 mm and an accelerating voltage of 3 kV. EDX was measured with an Ultim Extreme detector to evaluate the elemental composition of the samples. The spectra were evaluated with the Integrated Calibration and Application Tool (INCA) software (*Oxford Instruments*). The cryo-FIB (Zeiss Ion sculptor FIB-column; *Carl Zeiss Microscopy GmbH*) was employed to cut the Li-containing electrode at −150 °C to avoid Li melting. All sensitive samples were transferred with the vacuum-sealed holder to prevent air exposure.

The crystallinity and phase changes of the µ-Si electrodes were analyzed by in situ X-ray diffraction (*Bruker AXS GmbH*) with a Cu-K_α wavelength of 0.154 nm and a divergence slit of 0.5°. XRD analyses of the µ-Si electrodes were carried out using a homemade in situ cell with a 10 mm inspection area. The electrodes were prepared as described above, while the µ-Si composite material faced a beryllium (Be) disk (thickness: 250 µm; *Brush Wellmann GmbH*). The XRD measurements were conducted in the 2θ range from 10° to 40° with a step size of 0.05°. The XRD measurements started each 20 min for 48 h once the µ-Si electrodes were dropped with electrolyte (200 µL). After conducting the experiment, a full XRD pattern was recorded from 10° to 70° with a step size of 0.05°, from which the copper (110) reflection coming from the current collector was used for referencing the patterns.

Supporting Information

Supporting Information is available from the Wiley Online Library or from the author.

Acknowledgements

E.A. and M.M.B. contributed equally to this work. The authors thank the Ministry for Culture and Science of North Rhine Westphalia (Germany) for funding this work within the International Graduate School for Battery Chemistry, Characterization, Analysis, Recycling and Application (BACCARA). M.M.B. and M.C.S. acknowledge the financial support by the BMBF (Bundesministerium für Bildung und Forschung) within the ProLiFest (03XP0253A) project. The authors greatly acknowledge Andre Bar for his fantastic graphics support.

Open Access funding enabled and organized by Projekt DEAL.

Conflict of Interest

The authors declare no conflict of interest.

Data Availability Statement

The data that support the findings of this study are available from the corresponding author upon reasonable request.

Keywords

cell balancing, Ni-rich cathodes, prelithiation, silicon anodes, thermal evaporation

Received: September 27, 2022
Revised: November 7, 2022
Published online: November 27, 2022

[1] T. Placke, R. Kloepsch, S. Dühnen, M. Winter, *J. Solid State Electrochem.* **2017**, *21*, 1939.
[2] E. Adhitama, P. C. Rath, A. Prayogi, J. Patra, T.-C. Lee, J. Li, J.-K. Chang, *Carbon* **2021**, *184*, 752.
[3] M. Armand, P. Axmann, D. Bresser, M. Copley, K. Edström, C. Ekberg, D. Guyomard, B. Lestriez, P. Novák, M. Petranikova, W. Porcher, S. Trabesinger, M. Wohlfahrt-Mehrens, H. Zhang, *J. Power Sources* **2020**, *479*, 228708.
[4] R. Schmuch, R. Wagner, G. Hörpel, T. Placke, M. Winter, *Nat. Energy* **2018**, *3*, 267.
[5] M. N. Obrovac, V. L. Chevrier, *Chem. Rev.* **2014**, *114*, 11444.
[6] M. N. Obrovac, L. Christensen, *Electrochem. Solid-State Lett.* **2004**, *7*, A93.
[7] M. Winter, J. Besenhard, J. Albering, J. Yang, M. Wachtler, in *Progress in Batteries and Battery Materials*, Vol. *17* (Ed: L. Breveglieri), **1998**, p. 208.
[8] D. H. S. Tan, Y.-T. Chen, H. Yang, W. Bao, B. Sreenarayanan, J.-M. Doux, w. Li, B. Lu, S.-Y. Ham, B. Sayahpour, J. Scharf, E. A. Wu, G. Deysher, H. E. Han, H. J. Hah, H. Jeong, J. B. Lee, Y. S. Meng, *Science* **2021**, *373*, 1494.
[9] M. Marinaro, D. Bresser, E. Beyer, P. Faguy, K. Hosoi, H. Li, J. Sakovica, K. Amine, M. Wohlfahrt-Mehrens, S. Passerini, *J. Power Sources* **2020**, *459*, 228073.
[10] S. Dühnen, J. Betz, M. Kolek, R. Schmuch, M. Winter, T. Placke, *Small Methods* **2020**, *4*, 2000039.
[11] P. Meister, H. Jia, J. Li, R. Kloepsch, M. Winter, T. Placke, *Chem. Mater.* **2016**, *28*, 7203.
[12] V. L. Chevrier, L. Liu, D. B. Le, J. Lund, B. Molla, K. Reimer, L. J. Krause, L. D. Jensen, E. Figgemeier, K. W. Eberman, *J. Electrochem. Soc.* **2014**, *161*, A783.
[13] U. S. Vogl, S. F. Lux, E. J. Crumlin, Z. Liu, L. Terborg, M. Winter, R. Kostecki, *J. Electrochem. Soc.* **2015**, *162*, A603.
[14] M. Winter, W. K. Appel, B. Evers, T. Hodal, K.-C. Möller, I. Schneider, M. Wachtler, M. R. Wagner, G. H. Wrodnigg, J. O. Besenhard, *Chem. Mon.* **2001**, *132*, 473.
[15] E. Adhitama, S. Wickeren, K. Neuhaus, L. Frankenstein, F. Demelash, A. Javed, L. Haneke, S. Nowak, M. Winter, A. Gomez-Martin, T. Placke, *Adv. Energy Mater.* **2022**, *12*, 2201859.
[16] D. Vrankovic, M. Graczyk-Zajac, C. Kalcher, J. Rohrer, M. Becker, C. Stabler, G. Trykowski, K. Albe, R. Riedel, *ACS Nano* **2017**, *11*, 11409.
[17] H. Wu, G. Zheng, N. Liu, T. J. Carney, Y. Yang, Y. Cui, *Nano Lett.* **2012**, *12*, 904.
[18] W. Wu, Y. Kang, M. Wang, D. Xu, J. Wang, Y. Cao, C. Wang, Y. Deng, *J. Power Sources* **2020**, *464*, 228244.
[19] Y. Horowitz, H.-L. Han, F. A. Soto, W. T. Ralston, P. B. Balbuena, G. A. Somorjai, *Nano Lett.* **2018**, *18*, 1145.
[20] A. Schiele, B. Breitung, T. Hatsukade, B. B. Berkes, P. Hartmann, J. Janek, T. Brezesinski, *ACS Energy Lett.* **2017**, *2*, 2228.
[21] G. G. Eshetu, E. Figgemeier, *ChemSusChem* **2019**, *12*, 2515.
[22] F. Holtstiege, P. Bärmann, R. Nölle, M. Winter, T. Placke, *Batteries* **2018**, *4*, 4.
[23] T. Placke, G. G. Eshetu, M. Winter, E. Figgemeier, in *Lithium-Ion Batteries Enabled by Silicon Anodes*, (Eds: C. Ban, K. Xu), The Institution of Engineering and Technology (IET), United Kingdom, London **2021**, Ch. 11, p. 349.
[24] Y. Zhang, B. Wu, G. Mu, C. Ma, D. Mu, F. Wu, *J. Energy Chem.* **2022**, *64*, 615.
[25] C. Xin, J. Gao, R. Luo, W. Zhou, *Eur. J. Chem.* **2022**, *28*, e202104282.
[26] A. L. Michan, G. Divitini, A. J. Pell, M. Leskes, C. Ducati, C. P. Grey, *J. Am. Chem. Soc.* **2016**, *138*, 7918.
[27] R. Zhan, X. Wang, Z. Chen, Z. W. Seh, L. Wang, Y. Sun, *Adv. Energy Mater.* **2021**, *11*, 2101565.
[28] J. Betz, L. Nowak, M. Winter, T. Placke, R. Schmuch, *J. Electrochem. Soc.* **2019**, *166*, A3531.
[29] G. M. Overhoff, R. Nölle, V. Siozios, M. Winter, T. Placke, *Batteries Supercaps* **2021**, *4*, 1163.

[30] M.-T. F. Rodrigues, J. A. Gilbert, K. Kalaga, D. P. Abraham, *J. Phys. Energy* **2020**, *2*, 024002.
[31] Z. Wang, Y. Fu, Z. Zhang, S. Yuan, K. Amine, V. Battaglia, G. Liu, *J. Power Sources* **2014**, *260*, 57.
[32] Y. Li, B. Fitch, *Electrochem. Commun.* **2011**, *13*, 664.
[33] B. B. Fitch, M. Yakovleva, Y. Li, I. Plitz, A. Skrzypczak, F. Badway, G. G. Amatucci, Y. Gao, *ECS Trans.* **2007**, *3*, 15.
[34] P. Bärmann, M. Mohrhardt, J. E. Frerichs, M. Helling, A. Kolesnikov, S. Klabunde, S. Nowak, M. R. Hansen, M. Winter, T. Placke, *Adv. Energy Mater.* **2021**, *11*, 2100925.
[35] E. Adhitama, F. Dias Brandao, I. Dienwiebel, M. M. Bela, A. Javed, L. Haneke, M. C. Stan, M. Winter, A. Gomez-Martin, T. Placke, *Adv. Funct. Mater.* **2022**, *32*, 2201455.
[36] R. Nölle, K. Beltrop, F. Holtstiege, J. Kasnatscheew, T. Placke, M. Winter, *Mater. Today* **2020**, *32*, 131.
[37] X. Zhang, Z. Cui, A. Manthiram, *Adv. Energy Mater.* **2022**, *12*, 2103611.
[38] J. Guo, D. Dong, J. Wang, D. Liu, X. Yu, Y. Zheng, Z. Wen, W. Lei, Y. Deng, J. Wang, G. Hong, H. Shao, *Adv. Funct. Mater.* **2021**, *31*, 2102546.
[39] P. Bärmann, M. Diehl, L. Göbel, M. Ruttert, S. Nowak, M. Winter, T. Placke, *J. Power Sources* **2020**, *464*, 228224.
[40] D. S. M. Iaboni, M. N. Obrovac, *J. Electrochem. Soc.* **2015**, *163*, A255.
[41] J. Li, J. R. Dahn, *J. Electrochem. Soc.* **2007**, *154*, A156.
[42] J. C. Woodard, W. P. Kalisvaart, S. Y. Sayed, B. C. Olsen, J. M. Buriak, *ACS Appl. Mater. Interfaces* **2021**, *13*, 38147.
[43] F. Reuter, A. Baasner, J. Pampel, M. Piwko, S. Dörfler, H. Althues, S. Kaskel, *J. Electrochem. Soc.* **2019**, *166*, A3265.
[44] X. Wu, K. Song, X. Zhang, N. Hu, L. Li, W. Li, L. Zhang, H. Zhang, *Front. Energy Res.* **2019**, *7*, 1.
[45] V. L. Chevrier, L. Liu, R. Wohl, A. Chandrasoma, J. A. Vega, K. W. Eberman, P. Stegmaier, E. Figgemeier, *J. Electrochem. Soc.* **2018**, *165*, A1129.
[46] J. Kasnatscheew, T. Placke, B. Streipert, S. Rothermel, R. Wagner, P. Meister, I. C. Laskovic, M. Winter, *J. Electrochem. Soc.* **2017**, *164*, A2479.
[47] J. Li, L. E. Downie, L. Ma, W. Qiu, J. R. Dahn, *J. Electrochem. Soc.* **2015**, *162*, A1401.
[48] M. T. McDowell, S. W. Lee, W. D. Nix, Y. Cui, *Adv. Mater.* **2013**, *25*, 4966.
[49] J. Betz, G. Bieker, P. Meister, T. Placke, M. Winter, R. Schmuch, *Adv. Energy Mater.* **2018**, *9*, 1803170.
[50] B. R. Long, S. G. Rinaldo, K. G. Gallagher, D. W. Dees, S. E. Trask, B. J. Polzin, A. N. Jansen, D. P. Abraham, I. Bloom, J. Bareño, J. R. Croy, *J. Electrochem. Soc.* **2016**, *163*, A2999.